The Spatial Dimming Scheme for the MU-MIMO-OFDM VLC System

Zhen Feng*, *Student Member, IEEE*, Caili Guo†, *Senior Member, IEEE*, Zabih Ghassemlooy‡, *Senior Member, IEEE*, and Yang Yang*, *Student Member, IEEE*

**Beijing Laboratory of Advanced Information Networks, School of Information and Communication Engineering, Beijing University of Posts and Telecommunications, Beijing 100876, China*
†Beijing Key Laboratory of Network System Architecture and Convergence, School of Information and Communication Engineering, Beijing University of Posts and Telecommunications, Beijing 100876, China
‡Optical Communications Research Group, NCRLab, Faculty of Engineering and Environment, Northumbria University, Newcastle, UK
Email: fengzhen@bupt.edu.cn

Abstract: Multi-user visible light communication (MU-VLC) systems utilizing multiple-input multiple-output (MIMO) and orthogonal frequency-division multiplexing (OFDM) are gaining increased attentions recently. Visible light communication (VLC) links are expected to work under different illumination conditions and thus the need for dimming control mechanisms. However, the traditional analog and digital based dimming schemes have adverse effects on the data communications performance, such as clipping distortion and the variation of the duty cycle. In this paper, spatial dimming schemes based on the zero-forcing and the minimum mean-squared error precoding schemes are proposed for direct-current biased optical OFDM (DCO-OFDM) based indoor MU-MIMO VLC system, and the bipolar optical OFDM signal is biased by a fixed DC level. Transmit antenna selection (TAS) algorithms are designed for the optimum working LEDs subset at each dimming level. Owing to the simultaneously exploration of the selection diversity of light emitting diodes (LEDs)-based lights and the channel state information (CSI), the proposed spatial dimming schemes outperform the traditional dimming schemes, which is also verified by simulation results. Thus, the proposed schemes are shown to have a great potential to be applied in practical MU-MIMO-OFDM VLC systems.

Index Terms: Visible light communication (VLC), dimming control, multiple-input multiple-output (MIMO), orthogonal frequency-division multiplexing (OFDM), multiuser.

1. Introduction

Visible light communications (VLC) with a massive licensed free spectrum is being seen as a potential wireless technology as part of the fifth-generation (5G) and beyond wireless communication networks which can offer high-speed transmission data rates in indoor applications and to ease the pressure on the demand for bandwidth in radio frequency RF wireless systems [1].

However, the achievable data rate of VLC systems is usually constrained by the limited bandwidth (typically a few MHz) of off-the-shelf LEDs. In order to overcome this bandwidth (i.e., data rate) bottleneck several schemes have been proposed including: (*i*) multiple-input-multiple-output (MIMO), which utilize LEDs and multi-array photodiodes (PD) [2]; (*ii*) spectrally multi-carrier modulations such as orthogonal frequency-division multiplexing (OFDM) with data rate $>$ 4Gbps [3, 4], and multiband carrierless amplitude and phase (m-CAP) modulation, which is less complex with improved spectral efficiency compared with OFDM [5]; (*iii*) hybrid MIMO-OFDM and MIMO-m-CAP VLC systems with a spectral efficiency of 21.35b/s/Hz [6]; and (*iv*) multiuser MIMO (MU-MIMO), which can provide access to multiple users simultaneously [7]. The multi-user interference (MUI) in MU-MIMO VLC has adverse effects on communication, thus a number

of linear precoding schemes including zero forcing (ZF) [8] and minimum mean-squared error (MMSE) [9] have been proposed. The ZF precoding performs well under a high signal to noise ratio (SNR) level, whereas MMSE precoding offers improved tradeoff between the interference and the noise under ill-conditioned channels [7].

In indoor VLC systems data transmission should be facilitated under all illumination levels. Thus, the need for effective dimming control in VLC systems and in particular in MU-MIMO links with the sum-rate and the mean-square error (MSE) for ZF and MMSE precoding schemes, respectively. Note that, in the traditional dimming schemes the LED drive current is controlled by means of: (*i*) analogue dimming (AD) [4]; and (*ii*) digital dimming (DD) [10, 11]. More recently, a new type of dimming method known as spatial dimming (SD) was proposed in [12], where the illumination level was represented by the number of working LEDs in a LED-based light sources.

However, for MU-MIMO VLC systems with dimming, AD and DD schemes have some limitations, including: (*i*) the limited dynamic range of the LED especially at high or low dimming levels, since signal clipping will decrease the system performance [4], which is an issue in AD; and (*ii*) controlling the illumination level using a digital signal (i.e., pulse width modulation) with a variable duty cycle at cost of reduced data rate and increased complexity as in DD [13]. The SD scheme [12] is not applicable in multi-users dimming scenarios, since it merely selects LEDs with less optical power attenuation at each dimming level and therefore cannot be used to eliminate MUI. Therefore, the previous studies reported in the literature so far have not considered the specific characteristics of dimming control, MUI and LED nonlinearity in MU-MIMO-OFDM VLC systems. Against this background, in this paper we exploit the selection diversity of LED-based lights for dimming control. The main contributions of this paper are (*i*) novel designs of SD-ZF and SD-MMSE dimming schemes for the MU-MIMO-OFDM VLC system, by extending the work reported in [14]; (*ii*) analysis of the sum-rate reduction and MSE increasement in the proposed system as a function of the dimming level with the purpose to effectively suppress MUI; (*iii*) the use of transmit antenna selection (TAS) algorithms for the optimum operation of LEDs subset; and (*iv*) demonstrate by mean of simulation that the SD scheme can effectively mitigate clipping distortion compared with the traditional AD-based dimming schemes (i.e., AD-MMSE and AD-ZF), therefore the bit error rate (BER) and spectral efficiency of the system can be jointly improved.

The rest of the paper is presented as follows. The considered model of an indoor downlink MU-MIMO-OFDM VLC is outlined in Section 2, followed by the precoder design with the dynamic range constraint. The proposed SD-ZF and SD-MMSE schemes as well as the transmit antenna selection algorithms are introduced in Section 3. Simulation results and analysis are presented in Section 4, where the system performance is assessed and evaluated. Finally, concluding remarks are presented in Section 5.

Notation: Matrices and vectors are given by the bold uppercase and lowercase letters, respectively, $(\cdot)^T$ and $(\cdot)^\dagger$ represent the transpose and matrix pseudoinverse operations, respectively; $\mathbf{I}$ denotes an identity matrix; $\mathrm{E}\{\cdot\}$ is the expectation operation; $\min(a, b)$ computes the minimum of scalar *a* and *b*; $\mathrm{abs}(\cdot)$ denotes an element-wise absolute operator; and $|\mathbf{S}|$ is the size of a set S.

2. System Model

Fig. 1(a) illustrates the considered scenario for the indoor downlink MU-MIMO-OFDM VLC system, where an array of N_t-LED is used for illuminating a room as well as providing data communications to the *K*-user simultaneously. Note that, the user terminals (i.e., receivers (Rxs)) each with a single PD are placed on the floor and we have $Nt \geq K$.

2.1. Transmitter (Tx)

As shown in Fig. 1 (b), the input bits stream $b_i(t)$ (i.e., $b_i \in \{1, 0\}$) of each user is mapped into a group of complex *M*-ary quadrature amplitude modulation (*M*-QAM) symbols $D_{p,k}$ on each subcarrier, where $1 \leq p \leq K$ and $1 \leq k \leq N$, and *N* is the number of subcarriers. Note that, TAS algorithms can select n_t working LEDs from the LEDs array for dimming control, which will

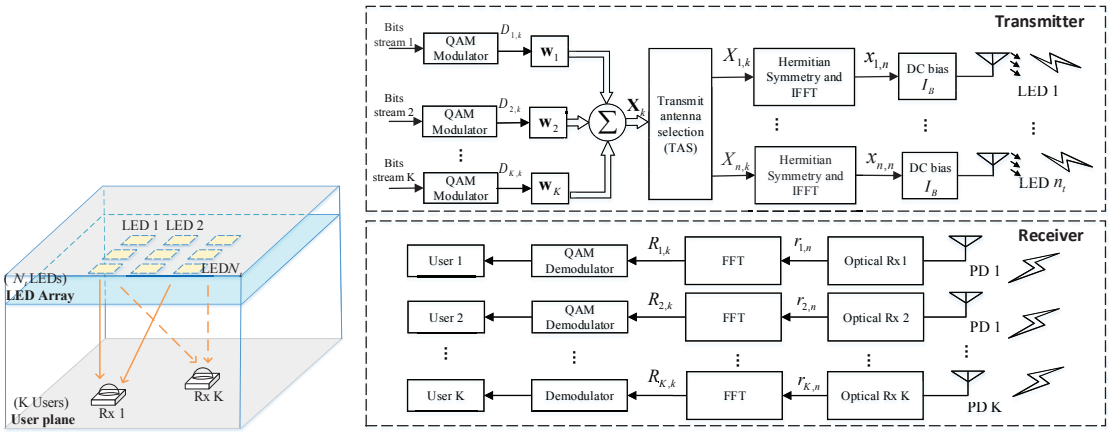

Fig. 1. MU-MIMO-OFDM VLC system: (a) the considered geometric scenario, and (b) block diagram for the downlink link with the proposed spatial dimming scheme.

be specified in Section 3. Then, the complex-valued QAM symbol $D_{p,k}$ will pass through a $n_t \times 1$ precoding vector $\mathbf{w}_k$, respectively. By summing all the precoded symbols from the *K*-user to the vector $\mathbf{X}_k$, the frequency-domain signal at the q^{th} Tx, which is also complex-valued, can be written as:

$$X_{q,k} = \sum_{p=1}^{K} w_{q,p} D_{p,k},\ k = 0,\ 1, ...,\ N-1, \tag{1}$$

Then Hermitian symmetry is applied to the precoded signal:

$$\begin{cases} X_{q,N-k} = X_{q,k}^{*}, & k = 1, 2, ..., N/2-1 \\ X_{q,0} = X_{q,N/2} = 0 \end{cases}. \tag{2}$$

Following the inverse fast Fourier transform (IFFT), the real-valued time-domain OFDM signal is obtained for subcarriers in (2):

$$x_{q,n} = \frac{1}{\sqrt{N}} \sum_{k=0}^{N-1} X_{q,n} \exp(j\frac{2\pi}{N} nk),\ n = 0, 1, ...N-1, \tag{3}$$

Note that, to further mitigate the inter-symbol interference (ISI), the cyclic prefix (CP) is included at the start of the time-domain OFDM symbol $\mathbf{x}_q = [x_{q,0}, x_{q,1}, ..., x_{q,N-1}]^T$. Finally, the electrical OFDM signal $x_{q,n}$ is DC-level shifted (i.e., the name DC-biased optical OFDM (DCO-OFDM)) prior to intensity modulation of the q^{th} LED.

With precoding, the emitted power (illumination) of the working LEDs will be different, which varies with the users moving around on the Rx plane. In order to provide data communications as well as a sufficient level of illumination simultaneously, we have adopted an unified DC bias level for working LEDs (i.e., same I_B) to ensure no clipping induced distortions. Note that, based on the central limit theorem, for $N \geq 64$, $x_{q,n}$ can be approximated as a Gaussian distribution with a very large absolute value [4]. To ensure operation within the dynamic range of LEDs it might be necessary to reduce the OFDM signal level, which may not be desirable (i.e., the problem of PAPR). Due to the non-linear electrical-to-optical characteristic, LEDs dynamic range is defined by $[I_l, I_h]$, where I_h and I_l are the maximum and minimum current levels, respectively. Note we have assumed that, the electrical-to-optical conversion coefficient is unity. Thus, the optical signal

following electrical-to-optical conversion can be expressed as:

$$y_{q,n} = \begin{cases} I_h, & if\ x_{q,n} \geq \frac{I_h - I_B}{a} \\ a \cdot x_{q,n} + I_B, & if \frac{I_h - I_B}{a} \geq x_{q,n} \geq \frac{I_l - I_B}{a} \\ I_L, & if\ x_{q,n} \leq \frac{I_l - I_B}{a} \end{cases}, \tag{4}$$

where a is a scaling factor adopted to maintain a constant clipping level per LED, which is given by:

$$a = \frac{\Delta I}{\sigma_x \sqrt{10^{\eta_{dB}/10} - 1}}, \tag{5}$$

where $\Delta I = \min(I_h - I_B, I_B - I_l)$, and $\eta_{dB} = 10\log_{10}(\eta^2 + 1)$dB is a factor to regulate the clipping level of the OFDM signal [4].

The human-perceived brightness merely responds to the average optical power instead of the instantaneous intensity of light signals.. For the q^{th} LED, the average optical power proportional to I_B, and is given by:

$$E[y_{q,n}] = E[ax_{q,n} + I_B] = I_B. \tag{6}$$

Since the QAM symbol $D_{p,k}$ is normalized to within [-1,1], following (4), the optical signal $y_{q,k}$, after precoding and DC biasing should satisfy:

$$-a\sum_{p=1}^{K}|w_{q,p}| + I_B \leq y_{q,n} \leq a\sum_{p=1}^{K}|w_{q,p}| + I_B. \tag{7}$$

To ensure that $y_{q,k}$ operates within the dynamic range $[I_l, I_h]$, we have:

$$\begin{cases} -a\sum\limits_{p=1}^{K}|w_{q,p}| + I_B \geq I_l \\ a\sum\limits_{p=1}^{K}|w_{q,p}| + I_B \leq I_h \end{cases} \tag{8}$$

Finally, based on (8), the following constraint is placed on the precoded signal $x_{q,n}$:

$$|x_{q,n}| = |\mathbf{W}\mathbf{D}_k|_q < \sum_{p=1}^{K}|w_{q,p}| <= \frac{\Delta I}{a} = \frac{d_0}{a} \tag{9}$$

2.2. VLC Channel

Typically, in most VLC links, the light signal arrives at the Rx via both line of sight (LOS) and non-LOS (i.e., diffuse) paths. For simplicity, we only consider the LOS path, which is assumed to be frequency flat and with the channel gain being the same for each subcarrier. This is a reasonable assumption considering that in VLC systems the indoor channel is a very static environment with very little variation in the intensity of the received signal (i.e., no fading in contrast to the RF wireless channels) [15]. In addition, we assume that perfect channel state information (CSI) is available at the Tx via either RF or other medium for the uplink (i.e., RF and infrared) as in [16].

For a LOS indoor VLC link the channel matrix is modeled as $\mathbf{H} \in \mathbf{R}^{K \times N_t}$, which is given by: $\mathbf{H} \in \mathbf{R}^{K \times N_t}$:

$$\mathbf{H} = \begin{bmatrix} h_{1,1} & \dots & h_{1,N_t} \\ \vdots & \ddots & \vdots \\ h_{K,1} & \dots & h_{K,N_t} \end{bmatrix}. \tag{10}$$

For the q^{th} Tx (i.e., LED) and the p^{th} Rx (i.e., user), the channel gain is given by [17]:

$$h_{p,q} = \begin{cases} \frac{(m+1)A}{2\pi d_{p,q}^2}\cos^m(\phi)g(\psi_{p,q})\cos(\psi_{p,q}) \\ \qquad\qquad , 0 \leq \psi_{p,q} \leq \Psi_c \\ 0 \qquad\qquad , \psi_{p,q} > \Psi_c \end{cases}, \tag{11}$$

where Lambertian emission order $m = \frac{-\ln(2)}{\ln(\cos(\Phi_{1/2}))}$ and $\Phi_{1/2}$ is the LED semi-angle at half illumination power. *A* represents the detector area and $d_{p,q}$ is the distance between the Tx and the Rx . ϕ is the angle of irradiance with respect to the Tx axis, and $g(\psi_{p,q})$ represents the gain of optical concentrator, which is given as:

$$g(\psi_{p,q}) = \begin{cases} \frac{\beta_p^2}{\sin^2(\psi_c)} & , 0 \leq \psi_{p,q} \leq \Psi_c \\ 0 & , \psi_{p,q} > \Psi_c \end{cases}, \tag{12}$$

where β_p denotes the refractive index and Ψ_c is the PD's field of view (FOV).

2.3. Receiver (Rx)

At the Rx, following photo-detection the DC bias is removed from the received signal and fast Fourier transform (FFT) is performed then in order to recover the frequency-domain symbols for the p^{th} user as given by:

$$\begin{aligned} R_{p,k} &= \sum_{q=1}^{N_t} H_{p,q} X_{q,k} + N_{p,k} \\ &= \mathbf{H}_p^T \mathbf{W}_p D_{p,k} + \sum_{l \neq p}^{K} \mathbf{H}_p^T \mathbf{W}_l D_{l,k} + N_{p,k},\ k = 0, 1, .., N-1 \end{aligned}, \tag{13}$$

where $\mathbf{H}_p$ is a $N_t \times 1$ channel vector for p^{th} user, $\mathbf{W}_p$ and $\mathbf{W}_l$ are $N_t \times 1$ vectors representing precoding weights, $N_{p,k}$ denotes the equivalent additive white Gaussian noise (AWGN) for the k^{th} subcarrier with zero mean and variance σ^2_{awgn}. Here the dominant noise sources considered are the shot noise and the thermal noise. Note that, in (13) the 1^{th} and the 2^{th} terms represent the desired signal and the inter-user interference, respectively.

3. MU-MIMO-OFDM VLC with SD

In dimmable downlink MU-MIMO-OFDM VLC systems, precoding schemes such as ZF and MMSE can be adopted to suppress MUI at each illumination level. The ZF-based scheme eliminates the interference by meeting the following condition:

$$\mathbf{HW} = diag\{[\mu_1, ..., \mu_K]^T\}, \tag{14}$$

where $\mu_p > 0,\ p = 1, ..., K$. Thus, the precoding matrix is given by:

$$\mathbf{W} = \mathbf{H}^{\dagger} diag\{[\mu_1, ..., \mu_K]^T\}, \tag{15}$$

where $\mathbf{H}^{\dagger} = \mathbf{H}^H(\mathbf{H}\mathbf{H}^H)^{-1}$.

Under ill-conditioned channel matrix, the ZF precoding scheme may severely reduce the signal-to-interference-plus-noise ratio (SINR) due to noise enhancement, thus deteriorating the system performance. Since noise becomes the dominant impairment not the interference, the MMSE precoding can balance the interference and the noise, with the precoding matrix given by:

$$\mathbf{W} = \mathbf{H}^H(\mathbf{H}\mathbf{H}^H + \sigma^2\mathbf{I})^{-1} diag([\mu_1, ..., \mu_K]^T), \tag{16}$$

where σ^2 denotes the variance of noise at the Rx.

In traditional AD schemes, I_B is usually adjusted for the required optical power level, since I_B proportional to the perceived brightness of human eyes. However, a combination of the optical DCO-OFDM signal with high PAPR and LED dynamic range will limit the signal clipping. Noted that, multiple LEDs are usually deployed in practice to ensure sufficient illumination level, and the user data streams are usually precoded at the Tx by which the complexity and power consumption of user terminals could be reduce. The SD scheme, which adjusts the number of working LEDs, can be applied as a more instinctive method for the downlink dimmable MU-MIMO-OFDM link, since the LEDs' selection diversity and the precoding matrix can be jointly optimized at the Tx.

Note that, we assume that the most modulated signals are within the dynamic range of LEDs and therefore the non-linearities between DC input and light output can be neglected [18]. Thus the dimming level is linearly proportional to the number of working LEDs in an LED lamp. Based on the above analysis, both SD-ZF and SD-MMSE are proposed for the MU-MIMO-OFDM VLC system. Since precoding is combined with the dimming control, the proposed schemes can effectively suppress the MUI, thus jointly improving the dimming and communication performance of the system.

The original state is defined by $\lambda = 100\%$ when N_t LEDs are glared and biased at the midpoint of LED's dynamic range, i.e., $I_0 = \frac{I_l+I_h}{2}$ is selected as the biasing level. Note that, the LEDs can be operated at higher biasing levels but at the cost of increase level of nonlinear induced distortion and upper clipping for the bipolar DCO-OFDM signal [19]. λ represents the normalized dimming level, which is given by:

$$\lambda = \frac{n_t}{N_t} \times 100\%. \tag{17}$$

Consequently, in the MU-MIMO-OFDM VLC system, $n_t = \lambda N_t$ LEDs are glared at dimming level λ. Although spatial dimming for a single-user MIMO VLC system and optical OFDM were proposed respectively [11, 12], little research has been presented in MU-MIMO-OFDM VLC systems. In addition, the impact of SD, more specifically, the number of working LEDs on data communications of the precoded MU-MIMO-OFDM VLC system needs investigating. In RF-based MU-MIMO systems with a given transmit power constraint, reducing the active transmit antennas will degrade the system performance (i.e., sum-rate and MSE) [20] and therefore TAS algorithms for ZF and MMSE precoding schemes are proposed. However, optical systems have two different features: (*i*) optical signals are real-valued and positive compared with the complex-valued RF signals; and (*ii*) the optical power is proportional to the current I in contrast to the electrical power is proportional to I^2. Therefore, the dedicated TAS algorithms are proposed for SD-MMSE and SD-ZF schemes-based VLC systems.

3.1. SD-ZF Scheme

Following the same approach in [21], the achievable data rate of MU-MIMO VLC is given by:

$$R = \sum_{p=1}^{K} \frac{1}{2} \log(1 + \frac{2\mu_p^2}{\pi e \sigma^2}). \tag{18}$$

Following (9), at each dimming level with n_t glared LEDs, the transmit power constraint in the electric domain is proportional to the number of working LEDs as given by:

$$P = tr(\mathbf{W}_S^H \mathbf{W}_S) < \frac{n_t d_0^2}{a^2} \tag{19}$$

where $\mathbf{W}_S$ is the ZF precoding matrix for selected working LEDs. Based on (15) and (19), we assume an identical gain factor μ for each user, which is expressed as $\mu^2 = \mu_p^2 = \frac{n_t d_0^2}{a^2 \cdot tr((\mathbf{H}_S^\dagger)^H \mathbf{H}_S^\dagger)} = \frac{n_t d_0^2}{a^2 \cdot tr(\mathbf{H}_S \mathbf{H}_S^H)^{-1}}$, where $\mathbf{H}_S$ denotes the $K \times n_t$ channel matrix, moreover $\mathbf{H}_S^\dagger = \mathbf{H}_S^H (\mathbf{H}_S \mathbf{H}_S^H)^{-1}$. Thus the sum-rate in (18) can be modified to:

$$R = \frac{K}{2} \log(1 + \frac{2 n_t d_0^2}{\pi e a^2 \sigma^2 tr(\mathbf{H}_S \mathbf{H}_S^H)^{-1}}). \tag{20}$$

For λ_0=100%, the original LEDs set is denoted as S', and S represents the desired selected working LED subset at the dimming level λ, where $|S'| = N_t$, $|S| = n_t = Nt \cdot \lambda$ and $S \subset S' \subseteq$

$\{1, 2, ..., N_t\}$. Then, the sum-rate degradation for λ can be obtianed from (20) as:

$$\begin{aligned} R_D(\lambda) &= R(\lambda_0) - R(\lambda) \\ &= \frac{K}{2}\log(1+\frac{2N_t d_0^2}{\pi e a^2\sigma^2 tr((\mathbf{H}_{S'}\mathbf{H}_{S'}^H)^{-1})}) - \frac{K}{2}\log(1+\frac{2n_t d_0^2}{\pi e a^2\sigma^2 tr((\mathbf{H}_S\mathbf{H}_S^H)^{-1})}) \\ &= \frac{K}{2}\log(1+M\cdot SNR\frac{tr(\mathbf{Q}_{S'})(1-\lambda)+tr(\mathbf{\Lambda}_{\bar{S}})}{(tr(\mathbf{Q}_{S'}))^2+tr(\mathbf{Q}_{S'})(tr(\mathbf{\Lambda}_{\bar{S}})+MN_t\lambda SNR)}) \end{aligned} \quad , \tag{21}$$

where $M=\frac{2}{\pi e}$, $SNR=\frac{N_t d_0^2}{a^2\sigma^2}$, $\mathbf{Q}_{S'}=(\mathbf{H}_{S'}\mathbf{H}_{S'}^H)^{-1}$, $\bar{S}=S'-S$ and $\mathbf{\Lambda}_{\bar{S}}=\mathbf{Q}_{S'}\mathbf{H}_{\bar{S}}(\mathbf{I}-\mathbf{H}_{\bar{S}}^H\mathbf{Q}_{S'}\mathbf{H}_{\bar{S}})^{-1}\mathbf{H}_{\bar{S}}^H\mathbf{Q}_{S'}$.

Then following the *Lemma 2* in [20] (13), $tr(\mathbf{\Lambda}_{\bar{S}})>0$, and finally we can prove that $R_D(\lambda)>0$, that is to say the sum-rate will decrease with dimming, equally with the reduced number of working LEDs. Moreover, for fixed $\mathbf{Q}_{S'}$ and SNR in (22), $R_D(\lambda)$ is shown to be monotonically increases with $tr(\Lambda_{\bar{S}})$ [20] (*Lemma 4*), which means that $R_D(\lambda)$ at λ can be minimized by reducing $tr(\Lambda_{\bar{S}})$. Therefore, the optimal working LEDs subset can be selected, which is given by:

$$S_{opt}=\arg\max_S R(S)=\arg\min_S R_D(\lambda)=\arg\min_S(tr(\mathbf{\Lambda}_{\bar{S}})). \tag{22}$$

Based on (22), the transmit antenna selection is performed on the original LEDs set S' iteratively for n_t working LEDs. During each cycle, LED with the minimum $tr(\Lambda_{\bar{S}})$ is removed from S'. Accordingly, $tr(\mathbf{\Lambda}_{\bar{S}})$ is simplified as $||h_r^H(\mathbf{H}_S\mathbf{H}_S^H)^{-1}||^2/(1-h_r^H(\mathbf{H}_S\mathbf{H}_S^H)^{-1}h_r)$. Therefore, the selection metric can be expressed as:

$$m=\arg\min_r \frac{||h_r^H(\mathbf{H}_S\mathbf{H}_S^H)^{-1}||^2}{(1-h_r^H(\mathbf{H}_S\mathbf{H}_S^H)^{-1}h_r)}. \tag{23}$$

Based on (23), and following [20] the proposed SD-ZF dimming scheme with TAS is shown in Algorithm 1.

Algorithm 1 : SD-ZF dimming scheme with TAS

Initialization: Set $n_t=\lambda N_t$; $S=\{1,2,...,N_t\}$; $|S|=N_t$; $\mathbf{H}_S=[h_1\ h_2\ ...\ h_{N_t}]$; $\mathbf{\Lambda}_S=(\mathbf{H}_S\mathbf{H}_S^H)^{-1}$.

Iteration:

1: **while** $|S|>n_t$ **do**

2: $m=\arg\min_r \frac{||\mathbf{h}_r^H\mathbf{\Lambda}_S||^2}{1-\mathbf{h}_r^H\mathbf{\Lambda}_S\mathbf{h}}$, where $r\in S$.

3: $\mathbf{\Lambda}_S=\mathbf{\Lambda}_S+\frac{\mathbf{\Lambda}_S\mathbf{h}_m\mathbf{h}_r^H\mathbf{\Lambda}_S}{1-\mathbf{h}_m^H\mathbf{\Lambda}_S\mathbf{h}_m}$.

4: $S=S-\{m\}$.

5: **end while**

Output:

The resulting set *S* and $\mathbf{W}_S=\mathbf{H}_S^H(\mathbf{H}_S\mathbf{H}_S^H)^{-1}diag\{[\mu_1,...,\mu_K]\}$ are desired working LEDs and precoding matrix at dimming level λ.

3.2. SD-MMSE Scheme

ZF precoding may amplify the noise at the Rx for the ill-conditioned channel matrix when the user is moving around within the room. Against this background, MMSE precoding is considered in this section, which can improve the SINR at the Rx with an trade-off between interference mitigation and the noise enhancement. Generally, the post-detection MSE of the MU-MIMO-OFDM VLC system can be expressed as:

$$\delta=\sum_{k=1}^{K}|R_{p,k}-D_{p,k}|^2. \tag{24}$$

Adopting a similar expression in [20], for λ with $\mathbf{H}_S$, the MSE can be expressed as:

$$\delta(S)=tr[(\alpha\mathbf{I}+\mathbf{H}_S\mathbf{H}_S^H)^{-1}], \tag{25}$$

where $\alpha = 1/SNR$. Therefore, the optimum working LEDs subset S_{opt} can be obtained by:

$$S_{opt} = \min_{S} \quad tr[(\alpha \mathbf{I} + \mathbf{H}_S \mathbf{H}_S^H)^{-1}]. \tag{26}$$

To evaluate the impact of SD on MSE, the difference of MSE compared with the original LED subset S' is derived as [20]:

$$\begin{aligned} \delta_D(\lambda) &= \delta(\lambda) - \delta(\lambda_0) \\ &= tr(\mathbf{A}_{S'} \mathbf{H}_{\bar{S}} (\mathbf{I} - \mathbf{H}_{\bar{S}}^H \mathbf{A}_{S'} \mathbf{H}_{\bar{S}})^{-1} \mathbf{H}_{\bar{S}}^H \mathbf{A}_{S'}) \end{aligned} , \tag{27}$$

where $\mathbf{A}_{S'} = (\alpha \mathbf{I} + \mathbf{H}_{S'} \mathbf{H}_{S'}^H)^{-1}$. Following the *Lemma 2* in [20], we can prove that $\delta_D(\bar{S}) > 0$, which reveals that when lower dimming level is required, the MSE will increase since fewer LEDs are glared. Therefore, to mitigate the performance loss, i.e., MSE enhancement, optimal working LEDs should be selected by:

$$S_{opt} = \arg\min_{S} \delta(\lambda) \equiv \arg\min_{S} |\delta_D(\lambda)| \ , \ |S| = \lambda N_t. \tag{28}$$

Based on (28), a TAS algorithm which minimizes the MSE enhancement is applied to iteratively select n_t working LED for required dimming level. During each cycle, one LED which minimize the $\delta_D(\lambda)$ in (27) is removed from S'. Thus $\delta_D(\lambda)$ can be reduced to $\left\|\mathbf{h}_r^H \mathbf{A}_S\right\|^2 / (1 - \mathbf{h}_r^H \mathbf{A}_S \mathbf{h}_r)$. Therefore, the selection problem is formulated as:

$$\arg\min_{r} \delta_D(r) = \arg\min_{r} \frac{\left\|\mathbf{h}_r^H \mathbf{A}_S\right\|^2}{1 - \mathbf{h}_r^H \mathbf{A}_S \mathbf{h}_r}. \tag{29}$$

Based on (29), and following [20] the proposed SD-MMSE dimming scheme with TAS is given in Algorithm 2.

Algorithm 2 : SD-MMSE dimming scheme with TAS

Initialization: Set $n_t = \lambda N_t$; $S = \{1, 2, ..., N_t\}$; $|S| = N_t$; $\mathbf{H}_S = [\mathbf{h}_1 \ \mathbf{h}_2 \ ... \ \mathbf{h}_{N_T}]$; $\mathbf{A}_S = (\alpha \mathbf{I} + \mathbf{H}_S \mathbf{H}_S^H)^{-1}$.

Iteration:

1: **while** $|S| > n_t$ **do**

2: $m = \arg\min_{r} \frac{||\mathbf{h}_r^H \mathbf{A}_S||^2}{1 - \mathbf{h}_r^H \mathbf{A}_S \mathbf{h}_r}$, where $r \in S$.

3: $\mathbf{A}_S = \mathbf{A}_S + \frac{\mathbf{A}_S \mathbf{h}_m \mathbf{h}_m^H \mathbf{A}_S}{1 - \mathbf{h}_m^H \mathbf{A}_S \mathbf{h}_m}$.

4: $S = S - \{m\}$.

5: **end while**

Output:

The resulting set *S* and $\mathbf{W}_S = \mathbf{H}_S^H (\mathbf{H}_S \mathbf{H}_S^H + \sigma^2 \mathbf{I})^{-1} diag([\mu_1, ..., \mu_K]^T)$ are the desired working LEDs and precoding matrix at dimming level λ.

3.3. Clipping Noise Analysis

LEDs have a limited dynamic range, and therefore the correct biasing is essential to ensure no saturation and clipping of the modulating signal, which could lead to harmonic and intermodulation distortion [22]. As for the clipping (i.e., the signal current $< I_l$) the induced distortion leads to the clipping noise with the variance given by [23] :

$$\begin{aligned} \sigma_{clip}^2 = \sigma_x^2 \{ & F - F^2 + \phi(\lambda_b)\lambda_b - \phi(\lambda_t)\lambda_t + [1 - Q(\lambda_b)\lambda_b^2] + Q(\lambda_t)\lambda_t^2 \\ & - [\phi(\lambda_b) - \phi(\lambda_t) + [1 - Q(\lambda_b)]\lambda_b + Q(\lambda_t)\lambda_t]^2 \} \end{aligned} , \tag{30}$$

where $\sigma_x^2 = tr(\mathbf{W}_S \mathbf{W}_S^H)/nt$ is the electronic power for each working LED, and $\phi(x) = \exp(-x^2/2)/\sqrt{2\pi}$ is probability density function (PDF). $F = Q(\lambda_b) - Q(\lambda_t)$ is an attenuation factor according to

Busggang theorem, where $Q(\cdot)$ is the complementary cumulative distribution function (CCDF), $\lambda_b = (I_B - I_l)/\sigma_x$, and $\lambda_t = (I_h - I_B)/\sigma_x$ is normalized bottom and top clipping levels respectively. Note that, the clipping noise experienced by the p^{th} user can be represented by:

$$\sigma^2_{clip,p} = \frac{\sigma^2_{clip}}{\sum\limits_{q=1}^{N_t} |w_{q,p}|^2}. \tag{31}$$

The users' clipping noise for the AD scheme can be obtained in a similar manner. Finally, based on (13) the effective SINR at Rx for the p^{th} user can be obtained:

$$SNDR_p = \frac{\left\|\mathbf{H}_p^T \mathbf{W}_p\right\|^2}{\sum\limits_{l=1, l\neq p}^{K} \left\|\mathbf{H}_p^T \mathbf{W}_l\right\|^2 + \sigma^2_{awgn,p} + \sigma^2_{clip,p}}. \tag{32}$$

4. Simulation Results

The simulation scenario for the proposed 4-QAM MU-MIMO-OFDM VLC system with 10×10 LED array, *K*=2 users, and 1024 OOFDM subcarriers is shown in Fig. 2 (a). In addition, a three-dimensional coordinate system is adopted, with the origin being at the middle of the floor, which is denoted by $\mathrm{O}(x, y, z) = (0, 0, 0)$. The position of both the LED arrays and the optical Rx are represented by their geometric centers with respect to the original point, respectively. The LEDs array pointing downward is installed on a plane 1.75m above the optical Rx of each user on the floor. The positions of users on the floor pointing upward are illustrated in Fig. 2 (b), where User 1 is fixed and User 2 have two different positions denoted as P1 and P2. The major system parameters employed in this paper are summarized in Table I.

For comparison, we compared the proposed SD scheme with AD. Note that, no comparison is made with DD, since signal detection for multiusers becomes too complex when considering a range of duty cycles [13]. The considered dimming schemes are as follows: (*a*) SD-MMSE - a SD scheme, where different number of working LEDS are selected for dimming control and MMSE precoding is adopted based on the CSI of the selected channel matrix $\mathbf{H}_S$; (*b*) SD-ZF - with MMSE precoding in SD-MMSE replaced by ZF precoding; (*c*) AD-MMSE - where I_B is adjusted for dimming control and the MMSE precoding matrix is derived from the entire LEDs subset; and (*d*) AD-ZF. It should be noted that, for the two AD schemes all the N_t LEDs are glared, and the 100% dimming level is defined when the biasing level is $I_{B,AD} = \frac{I_l + I_h}{2}$.

TABLE I
SYSTEM PARAMETERS FOR SIMULATION

Parameters	Notation	Values
Room size	$L \times W \times H$	4 m×4 m×3 m
LED array position	(*x*, *y*, *z*)	(0, 0, 2.5)
Number of users	*K*	2
Number of entire LEDs	N_t	100 (10×10)
Semiangle of half power	$\Phi_{1/2}$	60°
Distance of LED	D_t	0.1 m
Detect area of PDs	*A*	$1\ cm^2$
Bandwidth area of PDs	*B*	100 MHz
Field of view semiangle of the PD	Ψ_c	80°
Refractive index of optical concentrator	*n*	1.5
Height from Txs to Rxs	*h*	1.75 m

Firstly, we investigate the influence of clipping noise on the users. Based on (30) and (31), the clipping noise of User 2 as a function of the dimming level for η_{dB} of 3dB and 5dB is shown in Fig. 3, and the dynamic range is [0, 2]. Note that, SD-ZF and AD-ZF are compared herefor SD-MMSE

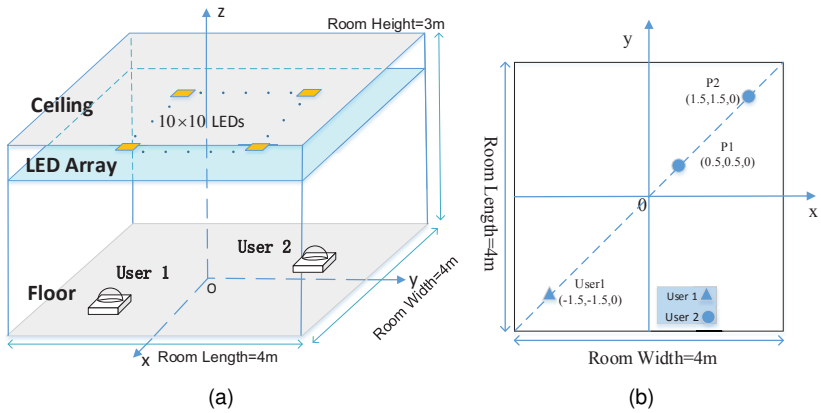

Fig. 2. (a) The room model used in the simulations, and (b) The configuration of user positions for scenarios A and B. Scenario A: User1 fixed, and User 2 fixed at P1; scenario B: User1 fixed, and User 2 fixed at P2.

and AD-MMSE the user's clipping noise can be obtained in a similar manner by replacing ZF with MMSE. For AD-ZF, $I_{B,AD} = \lambda I_0$ with N_t LEDs glared, the clipping noise shows a decreasing trend as the dimming level increases. While for SD-ZF the clipping noise is almost constant over the entire dimming range. In both cases, higher η_{dB} results in reduced clipping noise, this is because the signal will experience a lower clipping level.

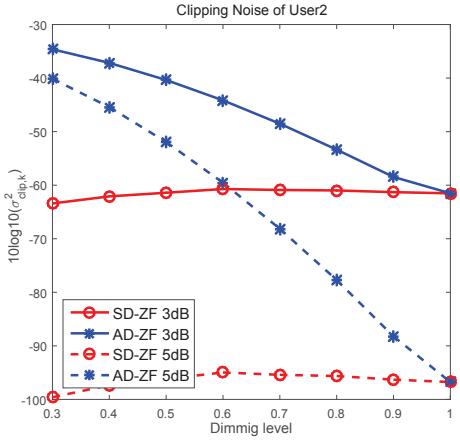

Fig. 3. The clipping noise versus the dimming level for the User2 for SD ZF and AD ZF schemes.

Secondly, we evaluate the BER performance with varied dimming levels in Fig. 4 by fixing SNR at 10 dB, 11 dB respectively. It should be noted that lower λ indicates fewer working LEDs for SD and lower biasing level for AD, and TAS algorithms are applied in SD schemes to recommend optimum working LEDs at each λ. It is observed that, the BER of all the considered dimming schemes decrease with λ, since increasing working LEDs can improve the performance of SD and higher bias level results in higher SNR in AD, which can improve the performance of SD and AD. Moreover, SD schemes display more flat plots. Since the TAS algorithms in SD can exploit the CSI and the selection diversity of working LEDs to compensate for the performance loss due dimming. In contrast, AD-MMSE and AD-ZF are much more susceptible to the variation of dimming levels.

Thirdly, we focus on the spectral efficiency for SD-based and AD-based schemes for a SNR of 10 dB, when the position of User 2 is fixed at P1. Based on (32), the aggregate achievable

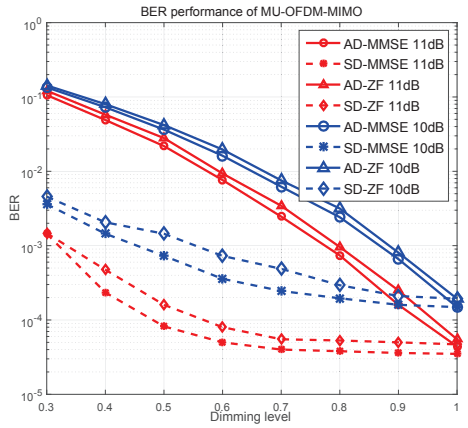

Fig. 4. The BER performance with different dimming levels for SD-MMSE, AD-MMSE, SD-ZF and AD-ZF schemes with different SNRs of 10 dB and 11 dB, and for the scenario A (User1 fixed, User 2 fixed at P1).

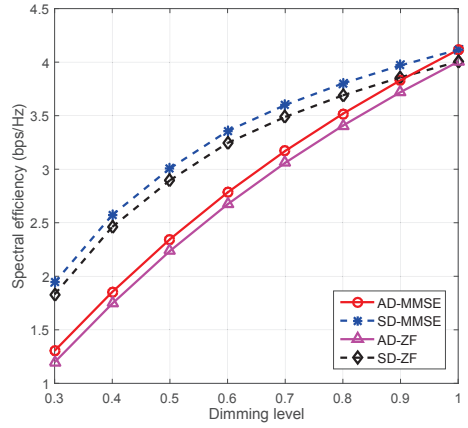

Fig. 5. Achievable spectral efficiency against dimming level for SD and AD schemes with the selected SNR of 10dB, and for the scenario A (User1 fixed, User 2 fixed at P1).

spectral efficiency based on Shannon capacity can be calculated with all effective SINRs at the Rxs [7]: $\sum_{p=1}^{K} \log(1+\mathrm{SINR}_p)$. As shown in Fig. 5, SD-MMSE and SD-ZF outperform AD-MMSE and AD-ZF for the considered dimming levels. This can be explained as follows. Compared with AD, SD schemes can effectively suppress the clipping noise exists in the OFDM transmission signal and increase SINR at the Rxs, therefore the higher spectral efficiency can be achieved. Further more, the SD-based scheme achieves higher spectral efficiency at higher dimming levels, since more LEDs are glared and the performance can be improved. In addition, SD-MMSE and AD-MMSE demonstrate improved performance over the ZF-based schemes (i.e., SD-ZF and AD-ZF), since MMSE precoding has higher SINR at the Rxs, which results in higher spectral efficiency.

Finally, we further investigate the influence of CSI imperfection in a realistic channel when users move to different positions as illustrated in Fig.2 (b) for λ=70%. User 1 is assumed to be stationary, while User 2 is moved from position P1 and P2, which indicates different correlation between the two users. In practical situations, CSI can be estimated at the Rx and fed back to the Tx via an uplink such as RF or infrared. Imperfect CSI will be induced by the quantized and noisy channel estimation, which is written by: $\mathbf{H} = \widehat{\mathbf{H}} + \Delta\mathbf{H}$ [9]. $\Delta\mathbf{H}$ denotes the CSI imperfection matrix the entries of which are independent Gaussian variables with variance σ_e^2. Fig.6 shows

the impact of imperfect channel estimation on the BER performance of SD and AD schemes. A normalized channel imperfection factor $\overline{\sigma_e} = \frac{\sigma_e}{\|vec(\mathbf{H})\|_1/(nt*Nr)}$ [9]. It can be observed that, the BER of SD and AD schemes deteriorate when $\overline{\sigma_e}$ is increased from 10^{-5} to 10^{0}, since MUI can not be suppressed by the precoder perfectly therefore lower SINR at the Rx. Besides, when User 2 at P2, the BER performance much improved compared with P1, since the channel condition will be less correlated when the two users are further separated. In addition, for $\overline{\sigma_e} > 10^{-2}$, the increase in BER for the SD-based scheme is more pronounced than AD-based schemes. Since SD schemes select the optimal working LEDs with the estimated CSI, its performance is more prone to the CSI imperfection.

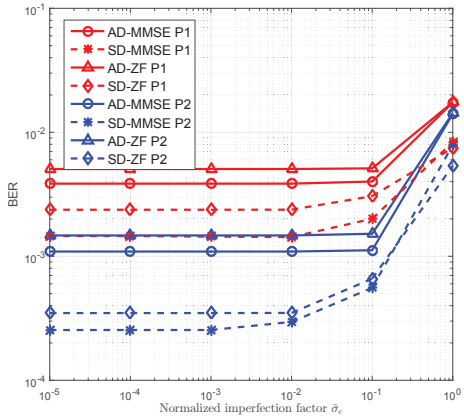

Fig. 6. Impact of channel imperfection on the BER performance of SD and AD schemes with the dimming level of 70%, and for different User2 positions at P1 and P2.

5. Conclusions

In this paper, SD-ZF and SD-MMSE dimming schemes were proposed for an indoor MU-MIMO-OFDM VLC system. We analyzed how the sum-rate and MSE performance are affected by spatial dimming in the MU-MIMO-OFDM VLC system, thus the tradeoff between the dimming control and communications performance. The TAS algorithms were applied to effectively suppress MUI and improve the system performance at the target dimming level. Compared with the traditional AD-based schemes, we showed that the proposed spatial dimming schemes could effectively suppress the signal-clipping distortion induced by LED's non-linearity and improve the system performance such as BER and spectral efficiency. These results revealed that, spatial dimming has a great potential to be adopted in practical MU-MIMO-OFDM VLC systems.

References

[1] P. H. Pathak, X. Feng, P. Hu, and P. Mohapatra, "Visible light communication, networking, and sensing: A survey, potential and challenges," *IEEE Communications Surveys Tutorials*, vol. 17, no. 4, pp. 2047–2077, Fourthquarter 2015.

[2] T. Q. Wang, C. He, and J. Armstrong, "Performance analysis of aperture-based receivers for mimo im/dd visible light communications," *Journal of Lightwave Technology*, vol. 35, no. 9, pp. 1513–1523, 2017.

[3] J. Armstrong and B. J. Schmidt, "Comparison of asymmetrically clipped optical ofdm and dc-biased optical ofdm in awgn," *IEEE Communications Letters*, vol. 12, no. 5, 2008.

[4] Y. Yang, Z. Zeng, J. Cheng, and C. Guo, "An enhanced dco-ofdm scheme for dimming control in visible light communication systems," *IEEE Photonics Journal*, vol. 8, no. 3, pp. 1–13, 2016.

[5] P. A. Haigh, A. Burton, K. Werfli, H. Le Minh, E. Bentley, P. Chvojka, W. O. Popoola,

I. Papakonstantinou, and S. Zvanovec, "A multi-cap visible-light communications system with 4.85-b/s/hz spectral efficiency," *IEEE Journal on Selected Areas in Communications*, vol. 33, no. 9, pp. 1771–1779, 2015.

[6] K. Werfli, P. Chvojka, Z. Ghassemlooy, N. B. Hassan, S. Zvanovec, A. Burton, P. A. Haigh, and M. R. Bhatnagar, "Experimental demonstration of high-speed $4\times$ 4 imaging multi-cap mimo visible light communications," *Journal of Lightwave Technology*, vol. 36, no. 10, pp. 1944–1951, 2018.

[7] Q. Wang, Z. Wang, and L. Dai, "Multiuser mimo-ofdm for visible light communications," *IEEE Photonics Journal*, vol. 7, no. 6, pp. 1–11, 2015.

[8] Z. Yu, R. J. Baxley, and G. T. Zhou, "Multi-user miso broadcasting for indoor visible light communication," in *Acoustics, Speech and Signal Processing (ICASSP), 2013 IEEE International Conference on*. IEEE, 2013, pp. 4849–4853.

[9] H. Ma, L. Lampe, and S. Hranilovic, "Coordinated broadcasting for multiuser indoor visible light communication systems," *IEEE Transactions on Communications*, vol. 63, no. 9, pp. 3313–3324, Sept 2015.

[10] J.-h. Choi, E.-b. Cho, Z. Ghassemlooy, S. Kim, and C. G. Lee, "Visible light communications employing ppm and pwm formats for simultaneous data transmission and dimming," *Optical and Quantum Electronics*, vol. 47, no. 3, pp. 561–574, 2015.

[11] Y. Yang, Z. Zeng, J. Cheng, and C. Guo, "Spatial dimming scheme for optical ofdm based visible light communication," *Optics express*, vol. 24, no. 26, pp. 30 254–30 263, 2016.

[12] Z. Wang, C. Guo, Y. Yang, and Q. Li, "A novel dimming scheme for indoor mimo visible light communication based on antenna selection," in *Vehicular Technology Conference (VTC Spring), 2016 IEEE 83rd*. IEEE, 2016, pp. 1–5.

[13] B. Li, R. Zhang, W. Xu, C. Zhao, and L. Hanzo, "Joint dimming control and transceiver design for mimo-aided visible light communication," *IEEE Communications Letters*, vol. 20, no. 11, pp. 2193–2196, 2016.

[14] Z. Feng, C. Guo, Y. Yang, Z. Ghassemlooy, and C. Feng, "Mmse based spatial dimming scheme for multiuser miso vlc systems," in *Globecom Workshops (GC Wkshps), 2017 IEEE*. IEEE, 2017, pp. 1–6.

[15] P. Chvojka, S. Zvanovec, P. A. Haigh, and Z. Ghassemlooy, "Channel characteristics of visible light communications within dynamic indoor environment," *Journal of Lightwave Technology*, vol. 33, no. 9, pp. 1719–1725, 2015.

[16] M. B. Rahaim, A. M. Vegni, and T. D. Little, "A hybrid radio frequency and broadcast visible light communication system," in *GLOBECOM Workshops (GC Wkshps), 2011 IEEE*. IEEE, 2011, pp. 792–796.

[17] T. Komine and M. Nakagawa, "Fundamental analysis for visible-light communication system using led lights," *IEEE transactions on Consumer Electronics*, vol. 50, no. 1, pp. 100–107, 2004.

[18] Q. Wang, Z. Wang, L. Dai, and J. Quan, "Dimmable visible light communications based on multilayer aco-ofdm," *IEEE Photonics Journal*, vol. 8, no. 3, pp. 1–11, 2016.

[19] R. Jiang, Q. Wang, F. Wang, L. Dai, and Z. Wang, "An optimal scaling scheme for dco-ofdm based visible light communications," *Optics Communications*, vol. 356, pp. 136–140, 2015.

[20] P.-H. Lin and S.-H. Tsai, "Performance analysis and algorithm designs for transmit antenna selection in linearly precoded multiuser mimo systems," *IEEE transactions on Vehicular Technology*, vol. 61, no. 4, pp. 1698–1708, 2012.

[21] H. Shen, Y. Deng, W. Xu, and C. Zhao, "Rate-maximized zero-forcing beamforming for vlc multiuser miso downlinks," *IEEE Photonics Journal*, vol. 8, no. 1, pp. 1–13, 2016.

[22] T. Zhang, Z. Ghassemlooy, S. Rajbhandari, W. O. Popoola, and S. Guo, "Ofdm-pwm scheme for visible light communications," *Optics Communications*, vol. 385, pp. 213–218, 2017.

[23] S. Dimitrov, S. Sinanovic, and H. Haas, "Clipping noise in ofdm-based optical wireless communication systems," *IEEE Transactions on Communications*, vol. 60, no. 4, pp. 1072–1081, 2012.